



OPEN

SUBJECT AREAS:

FLUORESCENCE
SPECTROMETRYCARBON NANOTUBES AND
FULLERENES

ELECTRON TRANSFER

ELECTRONIC PROPERTIES AND
MATERIALS

Empirical Prediction of Electronic Potentials of Single-Walled Carbon Nanotubes With a Specific Chirality (n,m)

Yasuhiko Hirana¹, Gergely Juhasz¹, Yuhei Miyachi^{2,3}, Shinichiro Mouri², Kazunari Matsuda² & Naotoshi Nakashima^{1,4,5}Received
24 April 2013Accepted
1 October 2013Published
16 October 2013

Correspondence and requests for materials should be addressed to N.N. (nakashima-tcm@mail.cstm.kyushu-u.ac.jp)

¹Department of Applied Chemistry, Graduate School of Engineering, Kyushu University, Motoooka 744, Fukuoka 819-0395, Japan, ²Institute of Advanced Energy, Kyoto University, Uji, Kyoto 611-0011, Japan, ³PRESTO, Japan Science and Technology Agency (JST), 4-1-8 Honcho Kawaguchi, Saitama 332-0012, Japan, ⁴International Institute for Carbon-Neutral Energy Research (WPH2CNER), Kyushu University, 744 Moto-oka, Nishi-ku, Fukuoka 819-0395, Japan, ⁵CREST, Japan Science and Technology Agency (JST), 5 Sanbancho, Chiyoda-ku, Tokyo, 102-0075, Japan.

The determination of the electronic states of single-walled carbon nanotubes (SWNTs) with a specific chirality has been a central issue in the science of SWNTs. Here we present the empirical equations with fitting parameters for the determination of the reduction and oxidation potentials of SWNTs for a wide range of diameters and chiral angles. In these equations, a distinct chirality family dependence of the reduction potentials is observed, while the oxidation potentials show a simple diameter dependence nearly proportional to the inversed nanotube diameter. Based on observations of the asymmetric chirality dependence between the reduction and oxidation potentials, the Fermi levels of the SWNTs were revealed to have a definite chirality family dependence, which indicates that the work functions of the SWNTs with small diameters deviate from the values for the large diameter SWNTs and graphene. We also performed quantum chemical calculations to compare the experiment to the calculations.

Due to their unique electronic properties and one-dimensional structure, single-walled carbon nanotubes (SWNTs) have attracted considerable attention as a promising nanomaterial for future nanoelectronics and nanophotonics¹⁻³. The SWNTs are a group of nanocarbon materials that have a cylindrical shape, but various chiralities. The chiral index (n,m) defines the nanotube diameter (d) and the chiral angle of the hexagons of the carbon atoms wrapped around its circumference. This index is the factor that determines the electronic properties of the SWNTs (i.e., electronic structure, Fermi levels, band gaps and redox potentials). *The determination of the electronic/redox potentials of the (n,m) SWNTs has been a central issue in the science and nanotechnology of carbon nanotubes.* Smalley and coworkers⁴ and Odom and coworkers⁵ reported the diameter-dependent band gaps of SWNTs using scanning tunneling microscopy and scanning tunneling spectroscopy. Redox titrimetry⁶, chemical doping⁷⁻⁹, and spectroelectrochemistry¹⁰⁻¹⁶ were employed to determine the redox potential of the individual (n,m) SWNTs. However, the achieved success in determining the redox potentials has been very limited¹⁷.

We have previously reported a photoluminescence (PL) spectroelectrochemical method that determines the precise redox potentials of individual (n,m) SWNTs (tube diameters (d) = 0.75–1.10 nm) embedded in a film of carboxymethylcellulose sodium salt (CMC-Na, Fig. S1a)¹⁷ (careful selection of the dispersant is important for fundamental and applied studies with soluble nanotubes^{18,19}). However, such an experimental method can only be applied to the (n,m) SWNTs whose diameters are small ($d < \sim 1.5$ nm) because the individual dissolution of the (n,m) SWNTs with $d > 1.5$ nm in a suitable polymer matrix, such as CMC-Na, is almost impossible. Even when we obtain such a film, it is difficult to detect an efficient PL intensity that allows a PL-spectroelectrochemical analysis for the determination of the precise redox potentials due to the low sensitivity of an IR-enhanced InGaAs detector. For a deeper understanding of the electronic properties, the determination of the precise reduction/oxidation potentials of the SWNTs with a wide range of diameters is quite important.

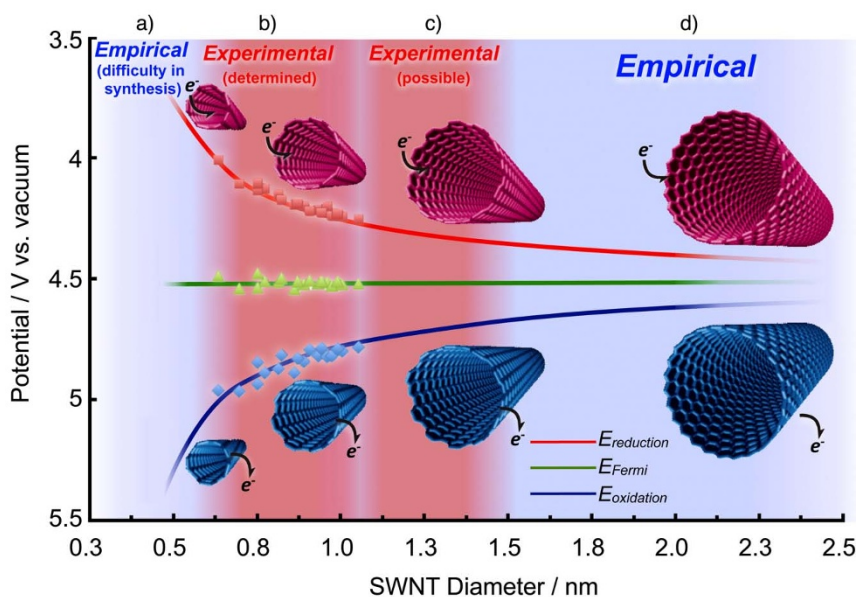


Figure 1 | The concept of this study. Experimental determination of the redox potentials of the SWNTs based on *in situ* PL electrochemical analysis is limited to the narrow diameter range (regions b and c) of the SWNTs; an empirical equation is needed in the ranges a and d due to i) the difficulty in synthesis of the SWNTs (region a), and ii) the very low sensitivity of an IR-enhanced InGaAs detector together with the difficulty in individual dissolution of the SWNTs (region d) that make *in situ* PL electrochemical analysis impossible.

Thus, it is essential to establish empirical correlations that predict the chirality/diameter dependent redox potentials of many (n,m) SWNTs. The chirality/diameter dependence of the redox potential becomes greater in SWNTs with small tube diameters. The concept of the study is presented in Figure 1, in which we recognize that experimental measurements of the redox potentials are possible only for a limited range of SWNT tube diameters, indicating the importance of the empirical correlation to evaluate their electronic states.

To achieve this objective, we first experimentally determined the redox potentials of (5,4)SWNTs ($d = 0.620$ nm), which are the SWNTs with the smallest tube diameter that we could obtain in a sufficient amount for the *in situ* PL spectroelectrochemical measurement. At the same time, in this study, we determined the redox states of the (6,4)- and (9,1)SWNTs whose diameters are 0.692 and 0.757 nm, respectively. Based on our previously reported data on redox potentials of 15 different (n,m) SWNTs¹⁷ and those of the 3 mentioned SWNTs measured in this study, we here present the chirality family dependent empirical equations that correlate the reduction (E_{red}) and oxidation (E_{ox}) potentials, Fermi levels (E_{F}) and work functions (WF) of the (n,m) SWNTs with a wide range of tube diameters.

We have discovered that based on these equations, the reduction potentials of the SWNTs show a clear chirality family dependence, while the oxidation potentials show no such noticeable chirality family dependence. We also performed quantum chemical calculations based on the Density Functional Tight Binding (DFTB) method to compare the experimentally determined redox values to the calculations.

Results

Determination of reduction and oxidation potentials, and Fermi level of the SWNTs. CoMoCAT SWNTs (Southwest NanoTechnologies) were solubilized by carboxymethylcellulose sodium salt (CMC-Na)^{17,20} (Supplementary Fig. S1), and a CMC-Na-solubilized SWNT film was fabricated on an ITO electrode based on our previous reports^{17,21}.

We recognized the isolated PL band from the (5,4)SWNTs ($d = 0.620$ nm) in the spectrum of the film measured using a Raman instrument (Supplementary Fig. S2). The chirality assignment is based on a report about the optical properties of the SWNTs with

small diameters²³. Based on the *in situ* PL spectral change as well as analysis using the Nernst equation, we determined the E_{red} , E_{ox} and E_{F} of the (5,4)SWNTs to be -0.59 , 0.75 and 0.08 V vs. Ag/AgCl, respectively. We also detected the PL signals mainly from five chiral indices of the SWNTs including (9,1), (8,3), (7,5), (6,5), and (6,4) ($d = 0.692$ – 0.829 nm) in the two-dimensional (2D)-map and 3D-surface PL plot of the SWNTs film (Supplementary Fig. S3). We carried out *in situ* PL spectroelectrochemical measurements of the (6,4)- and (9,1)SWNTs (their redox potentials have not yet determined) according to a previously described method¹⁷, and the results are shown in Supplementary Figs. S4–S7 together with those of three other SWNTs. The determined E_{red} , E_{ox} and E_{F} of the (5,4)-, (6,4)- and (9,1)SWNTs are summarized in Table 1, in which all the data were converted into a potential scale versus the vacuum level²², where E_{F} is defined as $(E_{\text{red}} + E_{\text{ox}})/2$.

Analysis of the diameter dependence of the electronic properties of the SWNTs. Together with the results previously reported for 15 different (n,m) SWNTs, we now have the redox potentials for a total of 18 different (n,m) SWNTs with the diameter range of 0.62–1.1 nm (Supplementary Fig. S8 and Table S1). In Fig. 2, E_{red} , E_{ox} and E_{F} are plotted as a function of the inverse nanotube diameter ($1/d$) using the data obtained from the 18 different (n,m) SWNTs. Both E_{red} and E_{ox} show an approximate linear dependence on $1/d$. The $1/d$ -dependent fitting lines for E_{red} and E_{ox} in the figure are consistent with the electronic structure of graphene, from which the electronic structures of the SWNTs can be deduced. However, as can be seen in the figure, E_{red} was found to exhibit a chirality family pattern just like the optical transition energies of the SWNTs^{24,25}. This tendency is different from the nanotube diameter dependence of E_{ox} ; namely E_{ox} shows no such distinct chirality family pattern, only simply proportional to $1/d$.

The E_{red} values of the $\text{mod}(2n + m, 3) = 1$ and 2-SWNTs are separated by the red fitting line, which corresponds to the line for the imaginary semiconducting SWNTs with the chiral angle $\theta = 30^\circ$ (hereafter referred to as the nominal armchair line) (Fig. 2). The $(2n + m) = \text{constant}$ family pattern of E_{red} is also clearly observed in Fig. 2 as shown by the gray lines. In these patterns, the smaller the chiral angles of the SWNTs, the greater the deviation of E_{red} from the



Table 1 | Experimentally determined electronic potentials of three (n,m)SWNTs in a CoMoCAT-SWNT sample

Chirality Index	Diameter/nm	E_{red}/V vs. vacuum	E_{ox}/V vs. vacuum	E_F/V vs. vacuum
(5,4)	0.620	3.85	5.19	4.52
(6,4)	0.692	3.85	5.05	4.45
(9,1)	0.757	3.89	5.01	4.45

nominal armchair line. This tendency is very similar to the well-known $(2n + m) = \text{constant}$ family patterns of the diameter dependence of the optical transition energy of the SWNTs^{24,25}. This result indicates the importance of the chiral angle for the empirical description of E_{red} . In order to consider the effect of the chiral angle, the E_{red} and E_{ox} were fitted using eq. 1 with the parameters provided in Table 2 as:

$$E = A + B/d + B'/d^2 + (C/d)\cos 3\theta + (C'/d^2)\cos 3\theta \quad (1)$$

where E is E_{red} , E_{ox} or E_F , and A , B , B' , C and C' are constants determined by this fitting procedures. These results are shown in Fig. 3 and Table 2. The calculated E_{red} and E_{ox} show good agreement

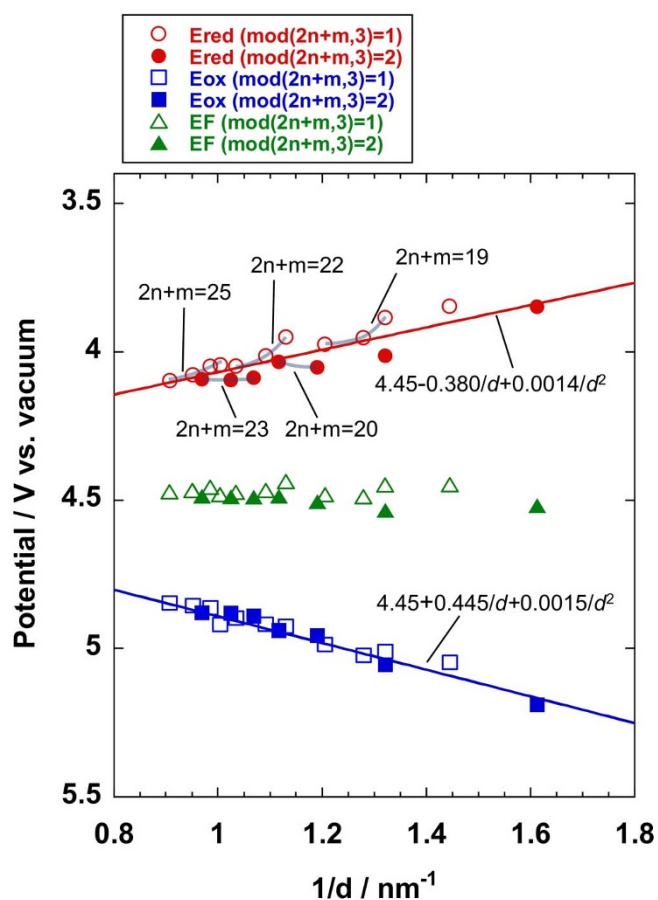


Figure 2 | Experimentally determined reduction potential, oxidation potential and Fermi level of (n,m)SWNTs. The experimentally determined reduction potential (E_{red}), oxidation potential (E_{ox}) and Fermi level (E_F) of 18 chiralities of the SWNTs are plotted as a function of the inversed nanotube diameter ($1/d$). The gray solid curve lines show $(2n + m) = \text{constant}$ family patterns. The red and blue solid lines are the fitting lines for E_{red} and E_{ox} of the armchair SWNTs, respectively. Red open circles: E_{red} of $\text{mod}(2n + m, 3) = 1$ -SWNTs. Red solid circles: E_{red} of $\text{mod}(2n + m, 3) = 2$ -SWNTs. Blue open squares: E_{ox} of $\text{mod}(2n + m, 3) = 1$ -SWNTs. Blue solid squares: E_{ox} of $\text{mod}(2n + m, 3) = 2$ -SWNTs. Green open triangles: E_F of $\text{mod}(2n + m, 3) = 1$ -SWNTs. Green solid triangles: E_F of $\text{mod}(2n + m, 3) = 2$ -SWNTs.

with the experimental data for the SWNTs for the wide range of diameters. Using these results, we predict E_{red} , E_{ox} and E_F of the SWNTs for a wide range of diameters ranging from ~ 0.6 – 3 nm (Fig. 4 and Supplementary Table S2; in this table, we selected 122 chiralities of the SWNTs with the range of diameters of 0.620–1.990 nm. For the plot of the redox states vs. SWNT diameters in the wide range of ~ 0.6 – 3.4 nm, see Supplementary Fig. S9), in which we see a distinct family pattern dependence for the reduction potential (E_{red}), while the oxidation potential (E_{ox}) does not show such a clear family pattern.

In addition to the experiments, we also performed calculations on the same set of nanotubes using the Density Functional based Tight Binding (DFTB) method. We used the band-structure around the Fermi level to predict the redox properties of the (n,m)SWNTs, and assumed a linear correlation of the energy of the conduction band minimum (CBM) and valence band maximum (VBM) with the oxidation and reduction potentials, respectively. This approach omits several important contributions to the redox potential, e.g., reorganization energies and solvent effect. However, the results show that the chirality family patterns and diameter dependence of the nanotube band structure still can reproduce most of the experimentally observed trends.

When the conduction and valence band energies are plotted as a function of the inverse diameters ($1/d$), the chiral family pattern is much more recognizable in the conducting band energies, while the valence band energies follows a smooth, quasi-linear $1/d$ dependence. Both this asymmetry and the calculated family pattern are in good agreement with the experimental data, in which only the reduction potentials show a characteristic chiral family pattern (see Supplementary Figure S11). The obtained similarities are even more pronounced when we compare the calculated band gaps with the electrochemical band gaps (see Supplementary Figures S12 and S13). The two values are very well correlated, and the calculated energy gap values systematically underestimate the experimental ones by about 0.1 eV.

Discussion

We initially discuss the accuracy of the empirical formula for E_{red} , E_{ox} , E_{elc} , and E_{ex} . The average relative errors for E_{red} , E_{ox} , E_{elc} , and E_{ex} were 0.3, 0.3, 1.4, and 0.8%, respectively. The results show that the fitting for E_{red} , E_{ox} , E_{elc} , and E_{ex} well reproduced the experimental data. Next, we discuss the range of applicability of the empirical formula. We expect that the empirical formula for the larger diameter range can be extrapolated with a good accuracy because the dispersion relation of the SWNTs with large diameters should be very similar to that of graphene and become a nearly linear function of $1/d$. On the other hand, for the smaller diameter range, we have observed the electronic potentials of the SWNTs with very small

Table 2 | Fitting parameters of eq. 1 for E_{red} and E_{ox} of SWNTs

E_{red} or E_{ox}	mod $(2n + m, 3)$	A	B	B'	C	C'
E_{red}	1	4.45	-0.380	0.00140	-0.0400	-0.00387
E_{red}	2	4.45	-0.380	0.00140	0.0717	-0.00197
E_{ox}	1	4.45	0.445	0.00150	-0.0155	-0.00364
E_{ox}	2	4.45	0.445	0.00150	-0.0354	0.00262

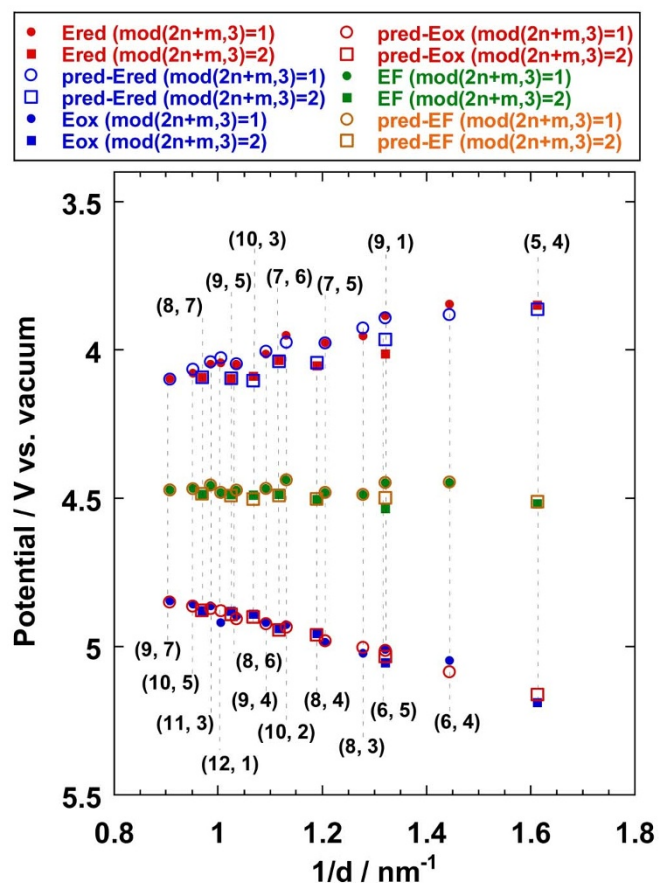


Figure 3 | Comparison between experimentally determined and predicted reduction potential, oxidation potential and Fermi level of (n,m) SWNTs. The experimentally determined and predicted reduction potential (E_{red}), oxidation potential (E_{ox}) and Fermi level (E_{F}) for the 18 chiralities of the SWNTs are plotted as a function of the inversed nanotube diameter ($1/d$). Red solid circles: E_{red} of $\text{mod}(2n+m,3) = 1$ -SWNTs. Red solid squares: E_{red} of $\text{mod}(2n+m,3) = 2$ -SWNTs. Blue open circles: predicted E_{red} of $\text{mod}(2n+m,3) = 1$ -SWNTs. Blue open squares: predicted E_{red} of $\text{mod}(2n+m,3) = 2$ -SWNTs. Blue solid circles: E_{ox} of $\text{mod}(2n+m,3) = 1$ -SWNTs. Blue solid squares: E_{ox} of $\text{mod}(2n+m,3) = 2$ -SWNTs. Red open circles: predicted E_{ox} of $\text{mod}(2n+m,3) = 1$ -SWNTs. Red open squares: predicted E_{ox} of $\text{mod}(2n+m,3) = 2$ -SWNTs. Green solid circles: E_{F} of $\text{mod}(2n+m,3) = 1$ -SWNTs. Green solid squares: E_{F} of $\text{mod}(2n+m,3) = 2$ -SWNTs. Orange open circles: predicted E_{F} of $\text{mod}(2n+m,3) = 1$ -SWNTs. Orange open squares: predicted E_{F} of $\text{mod}(2n+m,3) = 2$ -SWNTs.

diameters as shown in Table 1. These observations enabled us to construct a good empirical formula applicable for SWNTs with diameters as small as ~ 0.6 nm. For SWNTs with even smaller diameters ($d < 0.6$ nm), however, the fitting should not be applicable, because the π - and σ - orbitals of the carbon atoms should be significantly hybridized. In such a case, the energy dispersion relation of the SWNTs no longer simply inherits the dispersion relation of the graphene, and should exhibit a strong curvature effect that cannot be expressed by our empirical formula.

We now discuss how we can understand this apparently different family pattern of E_{red} and E_{ox} . It is known that the valence and conduction bands of graphene are nearly symmetric²⁶, and the energy dispersion relation of the SWNTs inherits the electron-hole symmetry of graphene. The reduction and oxidation potentials correspond to the conduction band bottom energy and valence band top energy, respectively. Hence, assuming that the Fermi energy is identical for all the (n,m) SWNTs, we expect a nearly symmetric

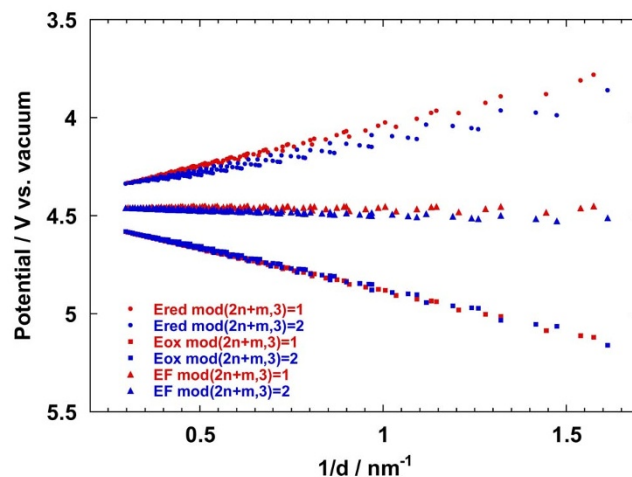


Figure 4 | Prediction of reduction and oxidation potentials and Fermi levels of (n,m) SWNTs. Predicted reduction potential (E_{red}), oxidation potential (E_{ox}) and Fermi level (E_{F}) of the 18 chiralities of the SWNTs are plotted as a function of the inversed nanotube diameter ($1/d$). Red circles: predicted E_{red} of $\text{mod}(2n+m,3) = 1$ -SWNTs. Blue circles: predicted E_{red} of $\text{mod}(2n+m,3) = 2$ -SWNTs. Red squares: predicted E_{ox} of $\text{mod}(2n+m,3) = 1$ -SWNTs. Blue squares: predicted E_{ox} of $\text{mod}(2n+m,3) = 2$ -SWNTs. Red triangles: predicted E_{F} of $\text{mod}(2n+m,3) = 1$ -SWNTs. Blue triangles: predicted E_{F} of $\text{mod}(2n+m,3) = 2$ -SWNTs.

family pattern for the E_{red} and E_{ox} ; however, as already described, the experimental data show a distinct family pattern only for E_{red} . The key to understanding this apparent paradox lies in the chirality family dependence of WF of the SWNTs. A previous theoretical study has predicted that the WF of SWNTs with diameters less than about 1 nm strongly depends on the specific chiral structure of the SWNTs²⁷. The WF and Fermi energy E_{F} are directly related, therefore, if the WF depends on the diameter and chiral angle, E_{F} may also depend on them.

The green circles and squares shown in Fig. 3 are the E_{F} values obtained from the experimentally determined E_{red} and E_{ox} . It was revealed that the E_{F} for the “mod = 1” family is always greater than those for the “mod = 2” family, especially for the small diameter SWNTs, and their deviation from the asymptotic value ($= 4.45$ eV) disappears for the larger diameter SWNTs. For the small diameter SWNTs, the deviation becomes significant. A similar tendency for the WFs of SWNTs with small diameters has been reported by Barone *et al.*²⁷ based on a theoretical study. They reported that the WF of the SWNTs with a diameter greater than 0.9 nm asymptotically and smoothly converges to the graphene limit of 4.6 eV. They also found that the WF of SWNTs with a smaller diameter exhibits a strong dependence on the diameter and chiral angle²⁷, in which the SWNTs of the $\text{mod}(2n+m,3) = 1$ family, such as the (6,4) SWNTs, have lower WFs in the diameter range of ~ 0.67 – 1.33 nm, which is consistent with our experimental observations. Therefore, we attributed the observed asymmetric behavior of E_{red} and E_{ox} to the chirality dependence of the WFs.

Finally, the electrochemical band gap, which is the difference between the E_{red} and E_{ox} , $E_{\text{elc}} = E_{\text{red}} - E_{\text{ox}}$, was evaluated. The previously reported empirical Kataura plot²⁵ describes the optical transition energy, which corresponds to the exciton energy E_{ex} . However, the electrochemical band gap obtained in this study corresponds to the one-electron band gap without an offset (binding energy) due to the excitonic effect. We fit E_{elc} using eq.1, which gives the empirical predictions of the band gaps of the SWNTs. The results are shown in Supplementary Fig. S10 and Table 3.

The results of the fitting contain important information on the electronic many-body effects in the SWNTs. We found that the



Table 3 | Fitting parameters of eq. 1 for electrochemical band gap (E_{elc}) and exciton energy (E_{ex}) of SWNTs

E_{elc} or E_{ex}	mod ($2n + m, 3$)	A	B	B'	C	C'
E_{elc}	1	0	0.825	0	0.0247	0
E_{elc}	2	0	0.825	0	-0.104	0.00220
E_{ex}	1	0.1	0.820	-0.015	0.0622	0.00523
E_{ex}	2	0.1	0.820	-0.015	-0.0110	-0.0532

constant A in eq.1 for the E_{elc} is zero, while we need a finite value of $A = \sim 0.10$ eV for the fitting of E_{ex} (Supplementary Fig. S10 and Table 3). The finite A value for the exciton energy is attributed to the many-body correction energy that only weakly depends on the tube diameter in the diameter range observed in this study²⁶. The coefficient B may correspond to the Fermi velocity of graphene and the electron hopping integral γ_0 between the nearest neighbor carbon atoms. We obtained $\gamma_0 = \sim 2.85$ eV from the coefficient B determined for E_{elc} . This value of γ_0 is close to the conventionally predicted value of the π -electron hopping integral for graphene and the SWNTs²⁸.

The observed values of E_{elc} are somewhat counter intuitive, because the quasi particle band gap in the intrinsic SWNTs is predicted to be strongly enhanced because of the many-body electronic correlation effects^{28,29}, which may lead to much higher values of E_{elc} than E_{ex} . The results thus imply that the electronic correlation energy at the electrochemically-doped sites on the SWNTs is strongly suppressed due to the screening by electrochemically injected electrons or holes and the dielectric response of the surrounding media with a very high dielectric constant (water), and the E_{elc} simply reflects the single particle hopping integral of the π -electrons.

The absence of the A coefficient for E_{elc} also indicates that there is no energy offset due to the many-body effect. In addition, in our previous study, we have found that the electrochemical band gaps of the SWNTs strongly depend on the dielectric constant of the materials surrounding the SWNTs²¹, which further supports the above understanding of the electrochemical band gaps. Recently, Spataru and Léonard³⁰ have theoretically predicted that the quasi particle band gap decreases with the increasing hole density in the SWNTs due to the additional screening effect induced by the doped holes. Therefore, our results are qualitatively consistent with the theoretical predictions of the band gap change under the doped conditions.

We carried out quantum chemical calculations based on the DFTB methods to compare the experimental data to the calculations and revealed the following two points:

- (i) The calculations are able to reproduce all the *important trends* that we observed in the electrochemical experiments, and confirm the new observations, such as the asymmetry of the chirality family dependence of the reduction and oxidation potentials.
- (ii) The accuracy of such calculations does not allow a high quality prediction of the redox properties at this point, therefore, they are not suitable to confirm the correctness of the suggested empirical relationship.

In conclusion, we established empirical equations that describe the dependence of the redox potentials of the SWNTs with a wide range of diameters and chiral angles. Without using the presented empirical equations, the determination of these potentials for SWNTs with larger diameters (>1.5 nm) is difficult or almost impossible. In this study, we discovered that the reduction potentials of the SWNTs showed a distinct chirality family dependence, while the oxidation potentials did not show such family pattern dependence. This difference is explained by the chirality family dependence of the WF of the SWNTs, and also confirmed by the theoretical calculations. These

calculations also showed that an accurate computational prediction of the redox properties is still a challenging task, therefore, empirical relationships between the structure and redox properties can be very useful and still have a strong predicting power. Finally, we would like to emphasize that the present study provides information on the fundamental properties of the SWNTs and graphene. This will lead to a deep understanding of their electronic states, which are essential for developing applications of these nanomaterials.

Methods

Materials. CoMoCAT-SWNTs, carboxymethylcellulose sodium salt (CMC-Na, Fig. S1a) and poly(diallyldimethylammonium chloride) (PDDA, Fig. S1b) were purchased from Southwest NanoTechnologies, Inc., Kishida Chemical and Aldrich, respectively, and were used as received. All other chemicals were of reagent grade and used as received.

Fabrication of modified electrode. The CoMoCAT-SWNTs (0.3 mg) were added to an aqueous solution (8 mL) of CMC-Na (0.1 wt%), and the mixture was sonicated (ultrasonic cleaner, Branson 5510) for 1 h, followed by ultracentrifugation at 150,000 g for 5 h. The SWNTs were individually solubilized in an aqueous solution of CMC-Na. A 100 μ L aliquot of the resultant solution was placed on a cleaned indium tin oxide-coated transparent quartz glass electrode (ITO) and then heated at ca. 100°C to obtain a SWNTs/CMC-Na film-modified electrode. A 100 μ L portion of an aqueous solution of PDDA (20 wt%) was then placed on the film followed by rinsing with water to remove any excess PDDA to obtain a SWNTs/CMC-Na/PDDA-modified electrode. PL spectroelectrochemistry was carried out using the obtained modified electrode.

PL and raman spectroelectrochemistry. Water was purified using a Milli-Q Plus Ultrapure water system coupled with an Elix-5 kit (Millipore Co.). Its resistivity was over 18 M Ω ·cm. The base electrolyte solution was 0.3 M aqueous NaCl containing 30 mM Na₂HPO₄ (pH 8). All the electrochemical measurements were conducted in an aqueous system using an Ag/AgCl (sat'd KCl) reference electrode and a coiled Pt wire counter electrode under an Ar gas atmosphere. The PL and Raman spectroelectrochemistry were carried out using a spectrofluorometer (HORIBA JOBIN YVON, FL3-21) and a Raman spectrophotometer (Kaiser Optical System, RXN) both equipped with a potentiostat (TOHO Technical Research Co., PS-06). The Raman scattering measurement was carried out at the excitation intensity of 10 mW.

Calculations. The calculations were performed using the DFTB+ program (ver 1.2) with the *mio* Slater-Koster set³¹. The nanotube models were calculated as the 3D periodic system with at least a 4.0 nm separation between the tubes in the x and y directions. The calculations were performed with the $2 \times 2 \times 8$ Monkhorst-Pack grid³². The unit cell size as well as the positions of the carbon atoms were optimized with a convergence criteria of 5 meV. The electronic converge criteria was 0.27 eV. Broyden mixing was applied with the mixing parameter of 0.2³³.

1. Avouris, P., Freitag, M. & Perebeinos, V. Carbon-nanotube photonics and optoelectronics. *Nat. Photon.* **2**, 341–350 (2008).
2. Lu, W. & Lieber, C. M. Nanoelectronics from the bottom up. *Nat. Mater.* **6**, 841–850 (2007).
3. Kim, S. N., Rusling, J. F. & Papadimitrakopoulos, F. Carbon nanotubes for electronic and electrochemical detection of biomolecules. *Adv. Mater.* **19**, 3214–3228 (2007).
4. Odom, T. W., Huang, J.-L., Kim, P. & Lieber, C. M. Atomic structure and electronic properties of single-walled carbon nanotubes. *Nature* **391**, 62–64 (1998).
5. Wilder, J. W. G., Venema, L. C., Rinzler, A. G., Smalley, R. E. & Dekker, C. Electronic structure of atomically resolved carbon nanotubes. *Nature* **391**, 59–62 (1998).
6. Zheng, M. & Diner, B. A. Solution redox chemistry of carbon nanotubes. *J. Am. Chem. Soc.* **126**, 15490–15494 (2004).
7. O'Connell, M. J., Eibergen, E. E. & Doorn, S. K. Chiral selectivity in the charge-transfer bleaching of single-walled carbon-nanotube spectra. *Nat. Mater.* **4**, 412–418 (2005).
8. Kim, S. M. *et al.* Reduction-controlled viologen in bisolvent as an environmentally stable n-type dopant for carbon nanotubes. *J. Am. Chem. Soc.* **131**, 327–331 (2008).
9. Kim, K. K. *et al.* Doping strategy of carbon nanotubes with redox chemistry. *New J. Chem.* **34**, 2183–2188 (2010).
10. Matsuda, K., Miyauchi, Y., Sakashita, T. & Kanemitsu, Y. Nonradiative exciton decay dynamics in hole-doped single-walled carbon nanotubes. *Phys. Rev. B* **81**, 033409 (2010).
11. Kazaoui, S., Minami, N., Matsuda, N., Kataura, H. & Achiba, Y. Electrochemical tuning of electronic states in single-wall carbon nanotubes studied by in situ absorption spectroscopy and ac resistance. *Appl. Phys. Lett.* **78**, 3433–3435 (2001).
12. Okazaki, K., Nakato, Y. & Murakoshi, K. Absolute potential of the Fermi level of isolated single-walled carbon nanotubes. *Phys. Rev. B* **68**, 035434 (2003).



13. Paolucci, D. *et al.* Singling out the electrochemistry of individual single-walled carbon nanotubes in solution. *J. Am. Chem. Soc.* **130**, 7393–7399 (2008).
14. Kavan, L. & Dunsch, L. Spectroelectrochemistry of carbon nanostructures. *Chem Phys Chem* **8**, 974–998 (2007).
15. Kalbac, M. *et al.* Electrochemical charging of individual single-walled carbon nanotubes. *ACS Nano* **3**, 2320–2328 (2009).
16. Kalbac, M. *et al.* Defects in individual semiconducting single wall carbon nanotubes: Raman spectroscopic and in situ Raman spectroelectrochemical study. *Nano Lett.* **10**, 4619–4626 (2010).
17. Tanaka, Y. *et al.* Experimentally determined redox potentials of individual (*n,m*) single-walled carbon nanotubes. *Angew. Chem. Int. Ed.* **48**, 7655–7659 (2009).
18. Kato, K., Inoue, A., Niidome, Y. & Nakashima, N. Thermodynamics on Soluble Carbon Nanotubes: How Do DNA Molecules Replace Surfactants on Carbon Nanotubes. *Sci. Rep.* **2**, 733 (2012).
19. Berber, M. R., Fujigaya, T., Sasaki, K. & Nakashima, N. “Remarkably Durable High Temperature Polymer Electrolyte Fuel Cell Based on Poly(vinylphosphonic acid)-doped Polybenzimidazole”. *Sci. Rep.* **3**, 1764 (2013).
20. Minami, N., Kim, Y., Miyashita, K., Kazaoui, S. & Nalini, B. Cellulose derivatives as excellent dispersants for single-wall carbon nanotubes as demonstrated by absorption and photoluminescence spectroscopy. *Appl. Phys. Lett.* **88**, 093123–093123 (2006).
21. Hirana, Y., Tanaka, Y., Niidome, Y. & Nakashima, N. Strong Micro-dielectric environment effect on the band gaps of (*n,m*) single-walled carbon nanotubes. *J. Am. Chem. Soc.* **132**, 13072–13077 (2010).
22. Kelly, C. P., Cramer, C. J. & Truhlar, D. G. Single-ion solvation free energies and the normal hydrogen electrode potential in methanol, acetonitrile, and dimethyl sulfoxide. *J. Phys. Chem. B* **111**, 408–422 (2007).
23. Miyata, Y. *et al.* Solution-phase extraction of ultrathin inner shells from double-wall carbon nanotubes. *ACS Nano* **4**, 5807–5812 (2010).
24. Kataura, H. *et al.* Optical properties of single-wall carbon nanotubes. *Synth. Met.* **103**, 2555–2558 (1999).
25. Weisman, R. B. & Bachilo, S. M. Dependence of optical transition energies on structure for single-walled carbon nanotubes in aqueous suspension: an empirical Kataura Plot. *Nano Lett.* **3**, 1235–1238 (2003).
26. Ando, T. The electronic properties of graphene and carbon nanotubes. *NPG Asia Mater.* **1**, 17–21 (2009).
27. Barone, V., Peralta, J. E., Uddin, J. & Scuseria, G. E. Screened exchange hybrid density-functional study of the work function of pristine and doped single-walled carbon nanotubes. *J. Chem. Phys.* **124**, 024709–024705 (2006).
28. Ando, T. Excitons in carbon nanotubes revisited: dependence on diameter, Aharonov–Bohm flux, and strain. *J. Phys. Soc. Jpn.* **73**, 3351 (2004).
29. Kane, C. L. & Mele, E. J. Electron interactions and scaling relations for optical excitations in carbon nanotubes. *Phys. Rev. Lett.* **93**, 197402 (2004).
30. Spataru, C. D. & Léonard, F. Tunable band gaps and excitons in doped semiconducting carbon nanotubes made possible by acoustic plasmons. *Phys. Rev. Lett.* **104**, 177402 (2010).
31. Elstner, M. *et al.* Self-consistent-charge density-functional tight-binding method for simulations of complex materials properties. *Phys. Rev. B* **58**, 7260 (1998).
32. Monkhorst, H. J. & Pack, J. D. Special points for Brillouin-zone integrations. *Phys. Rev. B: Solid State* **13**, 5188 (1976).
33. Johnson, D. D. Modified Broyden’s method for accelerating convergence in self-consistent calculations. *Phys. Rev. B: Condens. Matter* **38**, 12807 (1988).

Acknowledgements

The authors thank Prof. Kentaro Sato of Tohoku University and Prof. Andrew Robertson of Kyushu University for helpful discussions. This work was supported in part by the Low-Carbon Research Network (LCnet) and the Nanotechnology Platform Project (Molecules and Materials Synthesis) of the Ministry of Education, Culture, Sports, Science and Technology (MEXT), Japan.

Author contributions

N.N. proposed and supervised the project. Y.H. and G. J. carried out experiments and calculations, respectively. Y.H., G.J.Y.M., S. M., K.M. and N.N. wrote the manuscript.

Additional information

Supplementary information accompanies this paper at <http://www.nature.com/scientificreports>

Competing financial interests: The authors declare no competing financial interests.

How to cite this article: Hirana, Y. *et al.* Empirical Prediction of Electronic Potentials of Single-Walled Carbon Nanotubes With a Specific Chirality (*n,m*). *Sci. Rep.* **3**, 2959; DOI:10.1038/srep02959 (2013).



This work is licensed under a Creative Commons Attribution-NonCommercial-NoDerivs 3.0 Unported license. To view a copy of this license, visit <http://creativecommons.org/licenses/by-nc-nd/3.0>